

Intelligent Control Method of Power Supply for Tundish Electromagnetic Induction Heating System

Xinxing Xiang, An Luo, and Yan Li

Abstract—An intelligent control method is proposed to improve the performance of power supply for tundish electromagnetic induction heating, which can adequately regulate the tundish temperature. The topology structure of power supply for tundish electromagnetic induction heating is presented, and its working principle is analyzed. The power supply consists of six power units, and each of them consists of a fore-stage three-phase rectifier and back-stage single-phase inverter. The feed-forward control DC voltage is used by three-phase rectifier to obtain the stable DC voltage supplied to the inverter. The cloud controller based intelligent temperature control algorithm is combined with the power feed-forward algorithm to obtain accurate tracking of the output current and constant temperature control of the tundish steel in the back-stage inverter. The simulation and experiment are performed to verify the accuracy and effectiveness of the proposed method.

Index Terms—Cloud control, electromagnetic induction heating, rectifier-inverter, tundish.

I. INTRODUCTION

RECENTLY, with the progress of power electronics and semi-conductor technology, the emergence of high-power and high-efficient frequency conversion has significantly promoted the development of induction heating technology for steel heating. The practice of continuous casting technology indicates that the constant temperature casting with low superheat plays an important role in improving the quality and stable operation of a slab [1]-[4]. The input current of power supply for the tundish electromagnetic induction heating is the medium of power transformation and affects the power quality of public grids. Currently, its output relates to the temperature control of the tundish. The power supply for tundish electromagnetic induction heating is important for the production of special steel products in the continuous

casting process [5].

One of the most effective methods to improve productivity, solidification structure, and product quality corresponds to the control of the molten steel temperature of the tundish [6]-[8]. Therefore, more and more researchers focus on seeking an external heat source to compensate for the temperature drop of the steel water in the tundish, precisely control the optimal superheat, and keep the temperature of the steel water in the crystallizer stable. Therefore, various forms of power supply for electromagnetic induction heating system were developed in recent decades [9]-[13].

In [9], a topological structure of a low-loss voltage-type high-frequency series-load resonant inverter with an auxiliary switching capacitor unit was proposed. The conventional structure of power supply for tundish electromagnetic induction heating consists of a rectifier and series-resonant multi-inverter [14]. In [15], a simple D-class inverter with constant frequency was proposed for high-frequency induction heating. A new structure of a zero-voltage soft-switching high-frequency resonant inverter was proposed in [16]. The new power supply topologies, enabling high-performance induction heating by using the magnetic energy recovery, was proposed to add independent controllability of the frequency and current in [17]. A zero-voltage switching high-frequency resonant inverter with a load-power adaptive dual pulse modulated current phase controlled was presented for induction heating applications in [18]. Currently, most tundish heating power supply in China adopts the traditional topological structure, which is composed of multi-winding transformer, three-phase diode rectifier, and cascaded H -bridge converter. Specifically, AC/AC conversion from three-phase to single-phase can be easily realized. However, in the whole process of continuous casting, tundish exhibits thermal loss in varying degrees, especially during the abnormal casting periods such as the initial stage of casting, ladle exchange, and the end of casting, which inevitably leads to large temperature drop. Simultaneously, the steel water corresponds to nonlinear load, and its impedance varies with weight and temperature of the heated steel water. Most of electromagnetic induction heating power supplies are not treated well due to these factors [19], [20].

In this paper, an intelligent temperature control algorithm based on cloud controller is proposed, which can accurately

Manuscript received: January 30, 2019; accepted: July 27, 2019. Date of CrossCheck: July 27, 2019. Date of online publication: July 9, 2020.

This work was supported in part by the National Key Research and Development Program of China (No. 2016YFB0601302), and Science and Technology Major Programs of Hunan Province, China (No. 2016GK1002).

This article is distributed under the terms of the Creative Commons Attribution 4.0 International License (<http://creativecommons.org/licenses/by/4.0/>).

X. Xiang and A. Luo are with the Electrical and Information Engineering Department, Hunan University, Changsha, China (e-mail: zkdqxxx@163.com; an_luo@hnu.edu.cn).

Y. Li (corresponding author) is with the School of Automation, Central South University, Changsha, China (e-mail: liyanly@csu.edu.cn).

DOI: 10.35833/MPCE.2019.000066



track the output current of power supply for tundish electromagnetic induction heating and realize constant temperature control of the tundish steel water. Reactive power compensation is performed in the induction heating coil and capacitor, and the power factor of the power supply system is improved.

II. TOPOLOGY OF POWER SUPPLY FOR TUNDISH ELECTROMAGNETIC INDUCTION HEATING SYSTEM

The tundish electromagnetic induction heating system is powered by a high-power cascaded variable frequency power supply to the induction coil. Thereby, an electromagnetic field is formed, which generates a large current in the ladle to realize the heating of the molten steel. The topology of the tundish electromagnetic heating high-power cascaded variable frequency power supply is shown in Fig. 1. There are six power units. The fore-stage three-phase rectifier and back-stage single-phase full-bridge inverter are adopted in each power unit, which is supplied through the secondary winding of the transformer. The secondary winding is in delta connection to reduce input harmonic current. The modularization degree and redundancy of the whole power system are improved by adopting the modularization design concept of power units. It is very convenient to take out each power unit module from the rack and replace the same, which enhances the safety and reliability of the system. Conversely, when the power supply fluctuates, it ensures the stability of the DC-side voltage and increases the transmission density of the power unit.

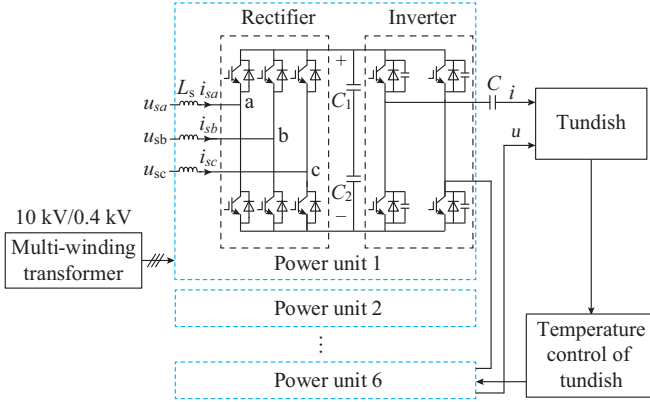


Fig. 1. Topology of power supply for tundish electromagnetic induction heating system.

In Fig. 1, L_s is the connection inductance on the AC input side; u_{sx} and i_{sx} , where $x = a, b, c$, are the three-phase AC input voltage and current, respectively; C_1 and C_2 are the series capacitors on the rectifier side; and C is the load-side reactive power compensation capacitor. Six power units are cascaded, and the carrier phase shift modulation strategy is adopted. We assume that the voltage of a sub-module corresponds to u_c , and the output voltage can be up to 27 levels from $-13u_c$ to $13u_c$.

III. CONTROL STRATEGY OF POWER SUPPLY FOR TUNDISH ELECTROMAGNETIC INDUCTION HEATING SYSTEM

The general control strategy of high-power-cascaded variable-frequency power supply for tundish electromagnetic induction heating system consists of the following three parts: the control for the fore-stage three-phase rectifier, the control for the back-stage full-bridge inverter, and the constant temperature control for the molten steel tundish. The corresponding control targets include the input current of the fore-stage rectifier, output load current of the back-stage inverter, and the temperature of the tundish, respectively.

A. Control of Fore-stage Rectifier

The power unit 1 in Fig. 1 can be used as a fore-stage rectifier circuit:

$$\begin{bmatrix} u_a \\ u_b \\ u_c \end{bmatrix} = \begin{bmatrix} u_{sa} \\ u_{sb} \\ u_{sc} \end{bmatrix} - L_s \frac{d}{dt} \begin{bmatrix} i_{sa} \\ i_{sb} \\ i_{sc} \end{bmatrix} \quad (1)$$

where u_a , u_b , u_c are the phase voltages of the inverter.

$$\begin{bmatrix} u_a \\ u_b \\ u_c \end{bmatrix} = u_{dc} \begin{bmatrix} s_{Ra} \\ s_{Rb} \\ s_{Rc} \end{bmatrix} \quad (2)$$

where s_{Rx} equals 1 and -1 for upper and lower bridge arm conductions, respectively.

The rectifier switching signals are expressed as:

$$\begin{bmatrix} s_{Ra} \\ s_{Rb} \\ s_{Rc} \end{bmatrix} = \frac{L_s}{u_{dc} T_s} \left\{ \begin{bmatrix} i_{sa}^*(k) \\ i_{sb}^*(k) \\ i_{sc}^*(k) \end{bmatrix} + \begin{bmatrix} i_{sa}(k) \\ i_{sb}(k) \\ i_{sc}(k) \end{bmatrix} \right\} + \frac{1}{u_{dc}} \begin{bmatrix} u_{sa}(k) \\ u_{sb}(k) \\ u_{sc}(k) \end{bmatrix} \quad (3)$$

where u_{dc} is the DC-side voltage in the rectifier; T_s is the switching period time of the insulated gate bipolar transistor; and k is discrete time. As shown in the above equations, the given input current signal of the rectifier shall be determined to obtain the switching signals of the rectifier.

The power P_s generated by the grid-side voltage of each power unit is equally distributed to each power unit and can be obtained as:

$$P_s = \frac{3U_s I_s}{2} \quad (4)$$

where U_s is the amplitude of the grid-side voltage of the power unit 1. The power P_L^* denotes the active power of the given load. Additionally, $P_s = P_L^*/6$. Hence, the amplitude of the rectifier input current I_s is as follows:

$$I_s = \frac{2P_L^*}{6 \times 3U_s} = \frac{P_L^*}{9U_s} \quad (5)$$

The tracking error Δu between the given DC-side voltage value u_{dc}^* and actual DC-side voltage value u_{dc} is obtained by the proportional integral (PI) regulator to obtain a DC-side current adjustment signal I_{dc}^* . The amplitude of the given input current of the rectifier is obtained as:

$$I_s^* = I_{dc}^* + I_s = \frac{P_L^*}{9U_s} + k_p \Delta u + k_i \int \Delta u dt \quad (6)$$

where k_p and k_i are the parameters of the PI. The currents of the AC-side of the fore-stage rectifier are then obtained by

$$\begin{bmatrix} i_a^* \\ i_b^* \\ i_c^* \end{bmatrix} = \left(\Delta I + \sqrt{\frac{P_L^*}{Z}} \right) \begin{bmatrix} \sin(\omega^* t) \\ \sin\left(\omega^* t - \frac{2}{3}\pi\right) \\ \sin\left(\omega^* t + \frac{2}{3}\pi\right) \end{bmatrix} \quad (12)$$

The reference output voltage u^* is divided by 6. This yields the following expression:

$$u_1^* = u_2^* = u_3^* = u_4^* = u_5^* = u_6^* = \frac{u^*}{6} \quad (13)$$

The reference output voltages of each power unit module u_1^* , u_2^* , u_3^* , u_4^* , u_5^* , u_6^* are obtained. Output voltage synchronization, power sharing, and redundant standby among the power unit are achieved in the control algorithm. The stability of the output voltage is improved.

2) Principle of Cloud Controller

Fuzzy theory can be applied to mathematically and precisely describe vague objects [21], [22]. Traditionally, a membership function of a fuzzy set is a one-to-one mapping from a space x to the unit interval [0,1]. Following the mapping, the uncertainty of an element belonging to the fuzzy concept becomes certain with a precise number. The uncertain characteristics of the original concept are not passed on to the next step of processing, which is not in accordance with the fuzzy thinking. However, with the model of membership clouds, soft computing can be implemented to exploit the tolerance and inheritance for the uncertainty and the imprecision or fuzziness and randomness [23].

The membership cloud is defined as follows. Let U be the set, $U = \{x\}$, as the universe of discourse. C is a linguistic term associated with U . The membership degree of x in U to the linguistic term C , $\mu(x) \in [0,1]$ is a random variable with a probability distribution. Subsequently, the distribution $\mu(x)$ denotes the membership cloud.

A membership cloud is a mapping from the universe of discourse U to the unit interval [0,1]. Thus, the mapping from all $x \in U$ to the interval [0,1] is a one-point to multi-point transition and produces a membership cloud as opposed to a membership curve. The concept of membership cloud provides qualitative and quantitative characterization of linguistic atoms. The definition of membership cloud effectively integrates the fuzziness and randomness of a linguistic term in a unified manner. In the cloud, fuzziness lies at the center, and it may not relate to the probability. However, a probability is adhered to the fuzziness from a statistical viewpoint [23], [24]. The degree of membership from x to C is a probability distribution as opposed to a fixed value.

The computation process of a cloud controller includes three steps, i.e., clouded numerical value, cloud uncertainty reasoning, and numerical cloud.

First, the numerical values are clouded. $R(E_x, \sigma)$ is assumed as a random function following a normal distribution, where E_x is the expected value and σ denotes the standard deviation. A normal random entropy with an expected value of E_n and a standard deviation of H_e is generated as:

$$E'_n = R(E_n, H_e) \quad (14)$$

where E'_n is the standard deviation; E_n is a measure of quali-

tative concept ambiguity which reflects the range of values accepted in the universe; and H_e is the entropy of E_n .

Then, a normal random number with the expected value of E_x and E'_n is generated as:

$$x_i = R(E_x, E'_n) \quad (15)$$

Finally, the membership function with the normal distribution form is obtained as:

$$\mu_i = \exp\left(\frac{-(x_i - E_x)^2}{2(E'_n)^2}\right) \quad (16)$$

where x_i is the cloud droplet that exhibits the degree of membership μ_i . A few cloud droplets form the cloud $G(E_x, E_n, H_e)$. A diagram of a cloud is shown in Fig. 4.

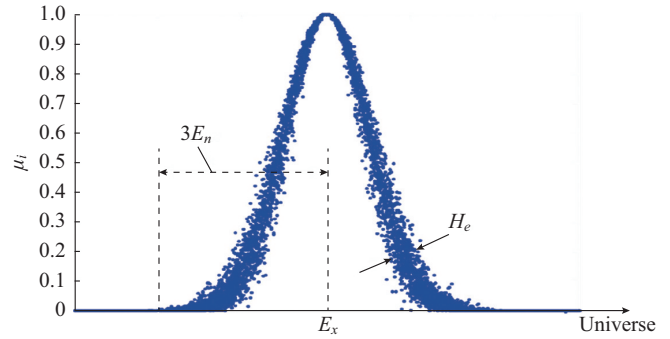


Fig. 4. Diagram of a cloud.

Based on the definition and Fig. 4, the degree of membership μ_i is not constant and always exhibits subtle changes. However, the changes do not affect the general characteristics of the cloud. The digital characteristics of the membership cloud are characterized by three values as follows: E_x , E_n , and H_e . The increases in E_n increase the range of values accepted by the concept, and make the concept more blurred. Additionally, H_e reflects the degree of dispersion of cloud droplets. The increases in the super entropy increase the dispersion of cloud droplets, the randomness of membership, and the “thickness” of the cloud [21]-[23]. It is proved that more than 99.74% of the cloud drops are scattered in the range $[E_x - 3E_n, E_x + 3E_n]$ [23], [25].

Second, the cloud uncertainty reasoning is done based on cloud generators. The cloud controller is composed of cloud generators, which includes the forward cloud generator and reverse cloud generator. If $G_A(E_x, E_n, H_e)$ is a one-dimensional normal membership cloud model and satisfies (14)-(16), it is termed as the forward one-dimensional cloud generator CG_A as shown in Fig. 5(a), where e and e_c are the deviation and the deviation difference of the input signal, respectively.

If $G_B(E_{xi}, E_{ni}, H_{ei})$ is a one-dimensional normal membership cloud model and satisfies the following expression:

$$E'_{ni} = R(E_{ni}, H_{ei}) \quad (17)$$

$$z_i = E_{xi} \pm \sqrt{-2 \ln(\mu(e, e_c))} E'_{ni} \quad (18)$$

Then three digital characteristic values include E_{xi} , E_{ni} , and H_{ei} . It is termed as the reverse one-dimensional cloud generator CG_B . When $e < E_{xe}$, the \pm in (18) is assumed as a nega-

tive sign. When $e > E_{xe}$, the \pm in (18) is assumed as a positive sign as shown in Fig. 5(b).

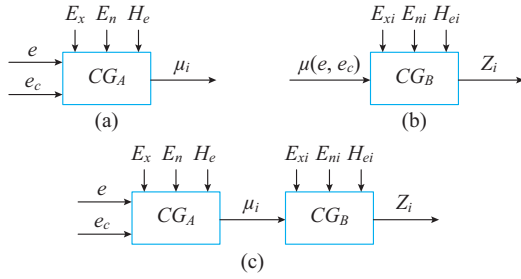


Fig. 5. Cloud generators and single-rule generator. (a) Forward cloud generator. (b) Reverse cloud generator. (c) Single rule generator.

The cloud uncertainty reasoning is based on cloud generators as shown in Fig. 5(c). A single rule can be described as if A then B . Additionally, A and B denote the qualitative language values.

Third, the resulting cloud is numerical. The numerical output can be obtained by the average value or the weighted average value of m cloud droplets z_i .

3) Cloud Controller for Tundish Steel Water Temperature Control

The deviation between the actual detected tundish molten steel temperature and the given temperature e and deviation difference e_c are used as input signals of the cloud controller. Based on different e and e_c , the cloud controller is used. ΔI of the back-stage inverter is then obtained.

The cloud model of e is represented by a numerical feature as $Ge(E_{xe}, E_{ne}, H_{ee})$. The cloud model of the deviation e_c is represented by a numerical feature as $Gec(E_{xec}, E_{nec}, H_{eec})$. In the paper, the golden section method [21] is used to generate seven clouds for the input signal, and this is used to denote the language value. Parameters of the forward one-dimensional cloud controller are shown in Table I.

TABLE I
PARAMETERS OF FORWARD ONE-DIMENSIONAL CLOUD CONTROLLER

Order	$Ge(E_{xe}, E_{ne}, H_{ee})$	$Gec(E_{xec}, E_{nec}, H_{eec})$	$Gp(E_{xp}, E_{np}, H_{ep})$
1	$Ge(-10, 3.3, 0.4)$	$Gec(-3, 0.9, 0.3)$	$Gp(-3, 0.1, 0.3)$
2	$Ge(-3.8, 2.1, 0.3)$	$Gec(-1.2, 0.6, 0.2)$	$Gp(-1.2, 0.6, 0.2)$
3	$Ge(-1.9, 1.3, 0.2)$	$Gec(-0.6, 0.2, 0.1)$	$Gp(-0.6, 0.2, 0.1)$
4	$Ge(0, 0.8, 0.1)$	$Gec(0, 0.4, 0.05)$	$Gp(0, 0.4, 0.05)$
5	$Ge(1.9, 1.3, 0.2)$	$Gec(0.6, 0.2, 0.1)$	$Gp(0.6, 0.2, 0.1)$
6	$Ge(3.8, 2.1, 0.3)$	$Gec(1.2, 0.6, 0.2)$	$Gp(1.2, 0.6, 0.2)$
7	$Ge(10, 3.3, 0.4)$	$Gec(3, 0.9, 0.3)$	$Gp(3, 0.1, 0.3)$

We consider the input signal deviation as an example. The seven cloud curves of e are shown in Fig. 6, and the number of cloud droplets per cloud is 1000.

The cloud controller implements a mapping relationship between the deviation input and controller output. A forward two-dimensional cloud generator and reverse one-dimensional cloud generator are used to construct qualitative rules with “and” conditions as shown in Fig. 7. The definitions of the forward two-dimensional cloud generator and reverse one-di-

mensional cloud generator are as follows.

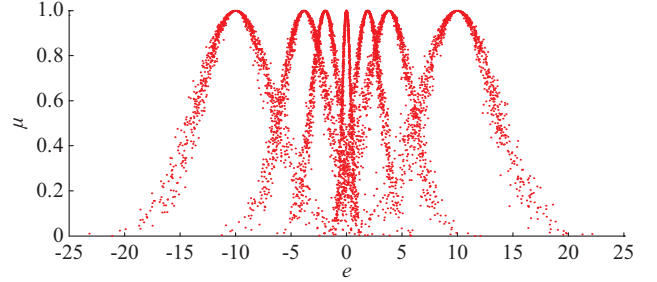


Fig. 6. Clouds of e .

The forward cloud generator is constructed using the three digital feature values of the cloud. If $G_A((E_{xe}, E_{xec}), (E_{ne}, E_{nec}), (H_{ee}, H_{eec}))$ is a two-dimensional normal membership cloud model and satisfies the following expression:

$$E'_{ne} = R(E_{ne}, H_{ee}) \quad (19)$$

$$E'_{nec} = R(E_{nec}, H_{eec}) \quad (20)$$

$$\mu(e, e_c) = \exp \left\{ \frac{-(e - E'_{xe})^2}{2E'_{ne}} + \frac{-(e - E'_{xec})^2}{2E'_{nec}} \right\} \quad (21)$$

Then, it is termed as the forward two-dimensional cloud generator CG_A .

The cloud controller proposed in the study consists of two-condition multi-rule uncertainty reasoning and the weighted average processing.

In Fig. 7, the input signals correspond to e and e_c , and the output corresponds to ΔI . Additionally, CG_A corresponds to a forward two-dimensional cloud generator, and CG_B corresponds to a reverse one-dimensional cloud generator.

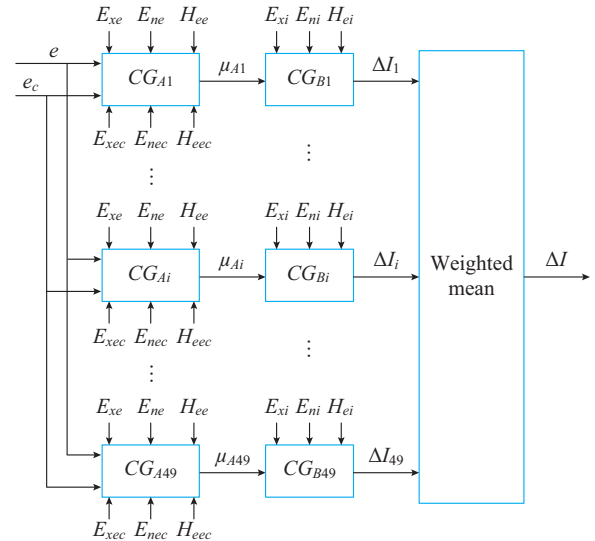


Fig. 7. Diagram of cloud controller with cloud generators.

As shown in Fig. 7, the reasoning part is realized by the forward cloud generator and reverse cloud generator. The cloud controller exhibits N ($N=49$) conditional rules, which is formalized as follows.

If $X = e$, $Y = e_c$, then $Z = \Delta I_i(\mu_{Ai})$. The input e and e_c stimu-

late different forward two-dimensional cloud generators CG_{A_i} to generate different μ_{A_i} . And μ_{A_i} then passes through CG_{B_i} to generate a large number of cloud droplets $\Delta I_i(\mu_{A_i})$, which are weighted and finally obtained. The output ΔI corresponds to the inputs e and e_c . We consider the weighted average of m cloud droplets as the output, which is expressed as:

$$\Delta I = \frac{\sum_{i=1}^m \Delta I_i \mu_{A_i}}{\sum_{i=1}^m \mu_{A_i}} \quad (22)$$

We substitute ΔI into (12), and the reference output current value of the heating power supply is finally obtained.

IV. SIMULATION AND EXPERIMENT

A. Simulation and Analysis

The simulation model of power supply for tundish electromagnetic induction heating system shown in Fig. 1 is established to verify the validity and accuracy of the control method proposed for power supply for tundish electromagnetic induction heating system. The AC-side voltage is 400 V and the frequency is 50 Hz. The number of cascaded modules is 6. The load current frequency is 200 Hz. The simulation results are shown in Fig. 8.

The input current waveform of the rectifier in the power unit 1 is shown in Fig. 8(a). The other power unit modules exhibit the same input current waveform. Figure 8(b) shows the DC-side voltage waveforms of the six power units. The DC-side voltage of each power unit remains stable with a deviation of approximately 5 V. Figure 8(c) shows the output power and its reference value, and the output power can stably track the reference value.

The power factor of the tundish is low. Thus, capacitor C is used to compensate the reactive power. The output voltage u and current i exhibit the same phase as shown in Fig. 8(d). The load is equivalent to a purely resistive load, which increases the power factor of the system.

B. Experiment and Analysis

The power supply for tundish electromagnetic induction heating system is developed and applied to a tundish induction heating device. Experiments are performed to verify the validity and accuracy of the proposed control method. The experimental results are shown in Fig. 9.

In Fig. 9(a), the input current of the rectifier in the power unit 1 exhibits a good waveform, and the input currents of other power units exhibit the same waveforms. Figure 9(b) shows the DC-side voltage waveforms of the six power units. The DC-side voltage of each power unit remains stable. Figure 9(c) shows the output power and its given reference value, and the output power can stably track the reference value. In Fig. 9(c), $P_{o,ref}$ is the rated load power and P_o is the load power. The output voltage u_o and current i_o exhibit the same phase as shown in Fig. 9(d), and the power factor is high.

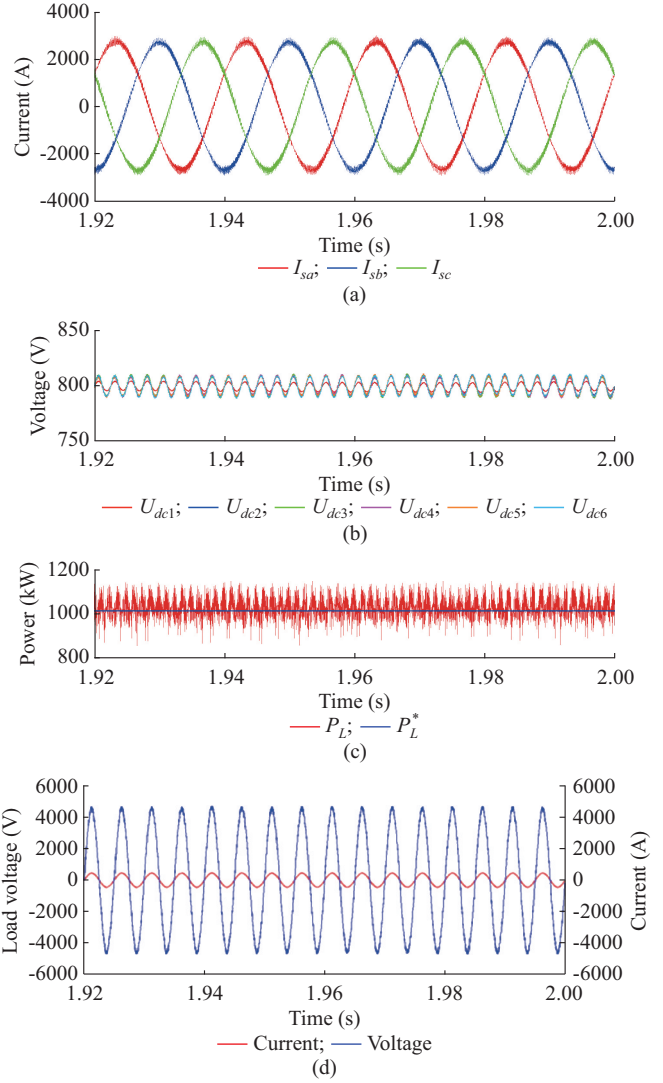


Fig. 8. Simulation results. (a) Fore-stage three-phase PWM input current. (b) DC-side voltages of each power unit. (c) Load power and given power. (d) Load voltage and load current.

V. CONCLUSION

We propose an intelligent control algorithm based on cloud control, which is applied to a tundish electromagnetic induction heating system. The topology structure of high-power-cascaded power supply for tundish electromagnetic induction heating system is given. The power supply consists of six power units, and each of them consists of a three-phase rectifier and a single-phase inverter. A stable DC voltage can be obtained from the three-phase rectifier that is supplied to the inverter. An intelligent control algorithm based on a cloud controller is proposed to control the temperature. The cascaded power supply can use the redundant standby module in a timely manner to stabilize the output when the module is faulty. Voltage synchronization, power sharing, and redundancy standby are achieved among the power modules. The simulation and experiment are performed separately. The results verify the accuracy and effectiveness of the proposed method.

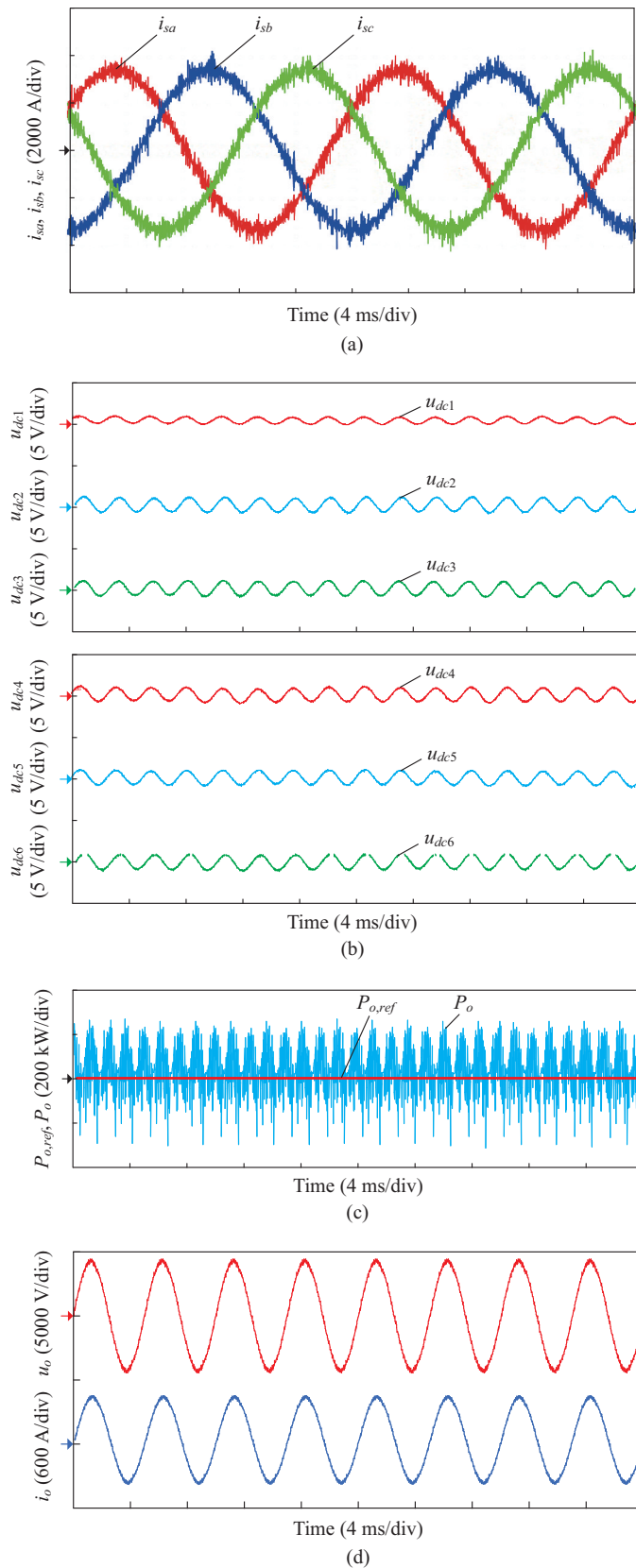


Fig. 9. Experimental result. (a) Three-phase PWM input current. (b) DC-side voltage. (c) Load power and given power. (d) Load voltage and load current.

REFERENCES

- [1] R. Li, Y. Li, D. Zhou *et al.* "The problem and application of tundish steel water plasma heating technology in China," *Steel*, vol. 34, no. 1, pp. 70-73, Jan. 1999.
- [2] B. Mao, J. Tao, and T. Jiang, "Continuous casting tundish channel induction heating technology," *Continuous Casting*, vol. 5, pp. 4-8, May 2008.
- [3] H. Pan, J. Zeng, G. Wu *et al.* "The development of tundish plasma heating technology," *Pangang Technology*, vol. 33, no. 4, pp. 5-8, Apr. 2010.
- [4] H. Sun, B. Zi, and J. Zhang, "Design and application status of continuous casting tundish channel type induction heating equipment," *Shanghai Metal*, vol. 34, no. 1, pp. 43-48, 2012.
- [5] D. J. Swinden, "Induction heating handbook," *Electronics and Power*, vol. 26, no. 8, pp. 665, Aug. 1980.
- [6] I. Suzuki, "Development of tundish induction heater for high quality continuously cast blooms," in *Proceedings of the 1988-71st Steelmaking Conference*, Toronto, Canada, Apr. 1988, pp. 125-131.
- [7] O. Lucía, P. Maussion, E. J. Dede *et al.* "Induction heating technology and its applications: past developments, current technology, and future challenges," *IEEE Transactions on Industrial Electronics*, vol. 61, no. 5, pp. 2509-2520, May 2014.
- [8] B. Saha and R. Y. Kim, "High power density series resonant inverter using an auxiliary switched capacitor cell for induction heating applications," *IEEE Transactions on Power Electronics*, vol. 29, no. 4, pp. 1909-1918, Apr. 2014.
- [9] O. Lucía, H. Sarnago, and J. M. Burdío, "Soft-stop optimal trajectory control for improved performance of the series-resonant multiinverter for domestic induction heating applications," *IEEE Transactions on Industrial Electronics*, vol. 62, no. 10, pp. 6251-6259, Oct. 2015.
- [10] V. Esteve, J. Jordán, E. Sanchis-Kilders *et al.*, "Comparative study of a single inverter bridge for dual-frequency induction heating using Si and SiC MOSFETs," *IEEE Transactions on Industrial Electronics*, vol. 62, no. 3, pp. 1440-1450, Mar. 2015.
- [11] H. Sarnago, O. Lucía, M. Pérez-Tarragona *et al.*, "Dual-output boost resonant full-bridge topology and its modulation strategies for high performance induction heating applications," *IEEE Transactions on Industrial Electronics*, vol. 63, no. 6, pp. 3354-3561, Jun. 2016.
- [12] A. Chakrabarti, A. Chakraborty, and P. K. Sadhu, "A fuzzy self-tuning PID controller with a derivative filter for power control in induction heating systems," *Journal of Power Electronics*, vol. 17, no. 6, pp. 1577-1586, Jun. 2017.
- [13] O. Lucía, H. Sarnago, and J. M. Burdío, "Soft-stop optimal trajectory control for improved performance of the series-resonant multi-inverter for domestic induction heating applications," *IEEE Transactions on Industrial Electronics*, vol. 62, no. 10, pp. 6251-6259, Oct. 2015.
- [14] V. Esteve, J. Jordán, E. Sanchis-Kilders *et al.*, "Comparative study of a single inverter bridge for dual-frequency induction heating using Si and SiC MOSFETs," *IEEE Transactions on Industrial Electronics*, vol. 62, no. 3, pp. 1440-1450, Mar. 2015.
- [15] T. Isobe and R. Shimada, "New power supply topologies enabling high performance induction heating by using MERS," in *Proceedings of the IECON 2013-39th Annual Conference of the IEEE Industrial Electronics Society*, Vienna, Austria, Nov. 2013, pp. 5046-5051.
- [16] T. Mishima and M. Nakaoka, "A load-power adaptive dual pulse modulated current phasor-controlled ZVS high-frequency resonant inverter for induction heating applications," *IEEE Transactions on Power Electronics*, vol. 29, no. 5, pp. 3864-3880, May 2014.
- [17] Z. Ma and A. Li, "Application of tundish type channel induction heating and refining technology in special steel continuous casting," in *Proceedings of the High Quality Steel Continuous Casting Production Technology and Equipment Exchange Meeting*, Changsha, China, Nov. 2014, pp. 520-523.
- [18] B. Mao and M. Wang, "Tundish induction heating and refining technology of tundish and its influence on continuous casting technology," in *Proceedings of the 2013 Continuous Casting New Technology and Key Durables Longevity Symposium*, Jinan, China, Jul. 2013, pp. 30-38.
- [19] V. Arredondo, M. A. Perez, and J. R. Espinoza, "Capacitor voltage ripple control based on decoupled power analysis in MMC," in *Proceedings of the IEEE 2017 11th IEEE International Conference on Compatibility, Power Electronics and Power Engineering*, Cadiz, Spain, Apr. 2017, pp. 544-549.
- [20] Y. Zhang, C. Qu, and J. Cao, "Performance improvement of direct power control of PWM rectifier under unbalanced network," *IEEE Transactions on Power Electronics*, vol. 32, no. 3, pp. 2319-2328,

Mar. 2017.

- [21] Rahul, K. Rajiv, and M. M. Tripathi, "Detection and classification of multiple power signal patterns with Volterra series and interval type-2 fuzzy logic system," *Protection and Control of Modern Power Systems*, vol. 2, no. 2, pp. 92-101, Feb. 2017.
- [22] N. Omar and I. Hamdan, "A novel controllable crowbar based on fault type protection technique for DFIG wind energy conversion system using adaptive neuro-fuzzy inference system," *Protection and Control of Modern Power Systems*, vol. 3, no. 3, pp. 328-339, Mar. 2018.
- [23] D. Li, D. Cheung, and X. Shi, "Uncertainty reasoning based on cloud models in controllers," *Computers & Mathematics with Applications*, vol. 35, no. 3, pp. 99-123, Mar. 1998.
- [24] D. Li, "Know ledge representation in KDD based on linguistic atoms," *Computer Science and Technology*, vol. 12, no. 6, pp. 481-496, Jun. 1997.

Xinxing Xiang received the B.E. degree from the School of Electronic Information, Wuhan University, Wuhan, China, in 2005. He is currently working towards the Ph.D. degree in the College of Electrical and Information

Engineering, Hunan University, Changsha, China. His research interests include electromagnetic induction heating technology, static var compensator and modular multilevel converter.

An Luo received the B.S. and M.S. degrees in industrial automation from Hunan University, Changsha, China, in 1982 and 1986, respectively, and the Ph.D. degree in fluid power transmission and control from Zhejiang University, Hangzhou, China, in 1993. Since 2003, he has been a Professor at Hunan University, Changsha, China, where he also serves as the Chief of National Electric Power Conversion and Control Engineering Technology Research Center. He was elected to the Chinese Academy of Engineering in 2015. His research interests include power conversion, harmonics suppression and reactive power compensation, and electric power saving.

Yan Li received her B.S., M.S., and Ph.D. degrees in automation, disaster prevention, and mitigation engineering and pattern recognition and intelligent system from Central South University, Changsha, China, in 1999, 2003, and 2007, respectively. She also performed research works in the electrical engineering post-doctoral research station of Hunan University, Changsha, China. Her current research interests include intelligent control, power quality, power control, and fault diagnosis of electrical machines.